Biogas Combustion in Premixed Flames or Electrochemical Oxidation in SOFC: Exergy and Emission Comparison

Francesco Quesito

Massimo Santarelli

Pierluigi Leone

Dipartimento Energia,
Politecnico di Torino,
10129 Torino, Italy

Suresh K. Aggarwal
University of Illinois at Chicago,
2039 ERF MC 251,
842 W. Taylor,
Chicago, IL 60607-7022

In the future energy pathway, characterized by flexibility of technologies and fuels, biogas could represent an alternative to conventional natural gas in feeding multiple types of technologies, both traditional thermal machines (chemical reactions), and innovative electrochemical generators such as fuel cells (electrochemical reactions). To compare the two pathways of energy production, two criteria are considered: (a) environmental analysis (emissions) and (b) exergy analysis. The results of the environmental and exergy comparison are presented and discussed in case of two selected transformation processes: partially premixed flames (PPFs, for chemical processes) and solid oxide fuel cells (SOFCs, for electrochemical processes), for a range of operating conditions. From an environmental point of view, the PPF exhaust stream has significant traces of NO_x and C_2H_2, which are precursors of atmosphere pollution, while the SOFC exhaust stream does not contain such chemical species due to the absence of combustion. From a exergy point of view, the utilisation of the biogas in form of electrochemical oxidation in a SOFC indicates significantly higher exergetic efficiency compared to the chemical oxidation in partially premixed flames. [DOI: 10.1115/1.4023173]

Keywords: biogas, premixed combustion, SOFC, modeling, exergy analysis, emission analysis

1 Introduction

Biogas represents a potentially important and renewable alternative to conventional natural gas in feeding multiple types of technologies apt to produce energy through both traditional and consolidated thermal machines (whose operation is based on a series of chemical reactions), as well as innovative electrochemical generators such as fuel cells (exploiting electrochemical reactions). Biogas could play an important role for both energy pathways, even though there are significant differences between them, which require investigations as to which of the two paths would lead to the best future perspectives.

In order to compare the above two pathways of energy production using biogas, two criteria are considered:

- emissions analysis
- exergy analysis

Exergy analysis is a powerful instrument for the comparison of the two conversion pathways to extract chemical exergy from a biogas stream. In terms of energy comparison, as the biogas primary fuel is used along different energy pathways, the energy product(s) of the transformation chain will be different in quantity and typology (e.g., mechanical power, heat flow at a given temperature, a stream of different chemical composition, etc.). Thus, a thermodynamic approach to homogenize different type of energy flows, allowing a quantitative comparison, is to make use of the concept of exergy.

Nevertheless, the exergetic approach is not able to get some other points of high value in the present energy context, as the emission of contaminants in atmosphere: therefore, the emission analysis is added as a complementary approach. For emission analysis, it is important to study the composition of the exhaust streams in terms of major components and contaminants. The stream composition can be computed models, which outline the composition in terms of the mole fractions of reactant (fuel and O_2), product (CO_2, H_2O, CO, H_2, intermediate hydrocarbons, etc.), and inert species, along with the traces of contaminants.

As examples of the methodology, the two processes considered in the paper are:

- Chemical process: partially premixed flames (PPFs), where fuel ignites by being premixed with compressed air inside a combustion chamber; this choice is due to the availability of previous existing literature (in particular, please consider Ref. [1]).
- Electrochemical process: solid oxide fuel cells (SOFCs), which can be fed via internal reforming of biogas by mixing it either with carbon dioxide (dry reforming) or water (steam reforming); a detailed numerical model has been developed and validated through experimental tests performed on a tubular anode-supported SOFC (with a detailed exhaust gas analysis through gas-chromatography, not described in the paper, but reported in Ref. [2]).

The results of the emissions and exergy comparison are presented and discussed for both PPFs and SOFCs, for a range of operating conditions.

2 Modeling

2.1 Biogas Combustion in Partially Premixed Flames. Governing equations for partially premixed flames rely on a similarity transformation that reduces the three-dimensional nature of the flow to a one-dimensional (axial) dependence of the governing
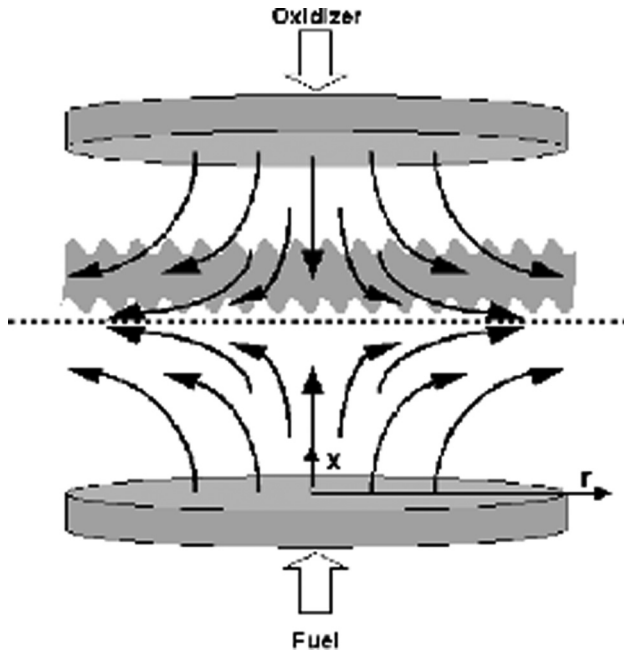
Fig. 1 Geometry of the axisymmetric opposed-flow diffusion flame. The dashed line represents the stagnation flame; the shaded region suggests the flame.

equations. This discussion pertains to the flame reactor model (OPPDIFF) in the Chemkin software.[1]

A steady-state solution is computed for axisymmetric partially premixed flames between two opposing nozzles. The configuration consists of two concentric, circular nozzles directed toward each other, as shown in Fig. 1. The two-dimensional axisymmetric flow is reduced mathematically to one dimension by assuming that the radial velocity varies linearly in the radial direction, which leads to a simplification in which the flow properties are functions of the axial distance only. The one-dimensional model then predicts the species, temperature, and velocity profiles in the core flow between the two nozzles (neglecting edge effects).

The reduction of the two-dimensional stagnation flow is based upon similarity solutions for incompressible flows performed by Kármán [3] and is more readily available in Schlichting [4]. The impinging and stagnation-flow models used in Chemkin are based on a finite domain, where the user specifies the nozzle separation distance. For this approach, an eigenvalue must be included in the solution of the equations, and the strain rate varies, such that a characteristic strain rate must be determined from the velocity profile. Following the analysis of Evans and Grief [5], Kee et al. [6] showed that this formulation allowed more accurate predictions of the extinction limits for premixed flames than other approaches. In the following equations, ξ represents the radial direction. A more detailed derivation of the governing equations for the opposed-flow geometry is provided by Kee et al. [6].

$$\frac{\partial(\rho u)}{\partial x} + \frac{1}{\xi}\frac{\partial(\rho v_\xi \xi)}{\partial \xi} = 0 \qquad (1)$$

where v_ξ is the radial or cross-flow velocity component. Following von Kármán [3], who recognized that v_ξ/ξ and other variables should be functions of the axial coordinate x only, we define:

$$G(x) = \frac{\rho v_\xi}{\xi} \qquad (2)$$

$$A(x) = \frac{\rho u}{2} \qquad (3)$$

Then the continuity Eq. (1) reduces to

$$G(x) = \frac{dA(x)}{dx} \qquad (4)$$

for the axial velocity u. Since A and G are functions of x only, so are ρ, u, T, and Y_k. The radial momentum equation is satisfied by the eigenvalue

$$H = \frac{1}{\xi}\frac{\partial p}{\partial \xi} = \text{const} \qquad (5)$$

The radial momentum equation is

$$H - 2\frac{d}{dx}\left(\frac{AG}{\rho}\right) + \frac{3G^2}{\rho} + \frac{d}{dx}\left[\mu\frac{d}{dx}\left(\frac{G}{\rho}\right)\right] = 0 \qquad (6)$$

Energy and species conservations are, respectively, implemented as follows:

$$\rho u\frac{dT}{dx} - \frac{1}{c_p}\frac{d}{dx}\left(\lambda\frac{dT}{dx}\right) + \frac{\rho}{c_p}\sum_k c_{pk}Y_k V_k\frac{dT}{dx} + \frac{1}{c_p}\sum_k h_k\dot\omega_k = 0 \qquad (7)$$

$$\rho u\frac{dY_k}{dx} + \frac{d}{dx}(\rho Y_k V_k) - \dot\omega_k W_k = 0 \quad k = 1,...,K \qquad (8)$$

Here, the diffusion velocities are given by the mixture-averaged formulation

$$V_k = -\frac{1}{X_k}D_{km}\frac{dX_k}{dx} - \frac{D_k^T}{\rho Y_k}\frac{1}{T}\frac{dT}{dx} \qquad (9)$$

where

$$D_{km} = \frac{1 - Y_k}{\sum_{j\neq k}^{K}\frac{X_j}{D_{jk}}} \qquad (10)$$

and D_{km}, D_{jk}, and D_k^T are the mixture-averaged, binary, and thermal diffusion coefficients, respectively. The boundary conditions for the fuel and oxidizer streams at the nozzles are

$$x = 0: \quad A = \frac{\rho_F u_F}{2}; \quad G = 0; \quad T = T_F;$$
$$\rho u Y_k + \rho Y_k V_k = (\rho u Y_k)_F \qquad (11)$$

$$x = L: \quad A = \frac{\rho_O u_O}{2}; \quad G = 0; \quad T = T_O;$$
$$\rho u Y_k + \rho Y_k V_k = (\rho u Y_k)_O \qquad (12)$$

The inflow boundary condition (12) specifies the total mass flux, including diffusion and convection, rather than the specifying the species mass fraction $Y_k = Y_{k,F}$. If gradients exist at the boundary, these conditions allow diffusion into the nozzle. The differential Eqs. (4)–(8) along with boundary conditions (11) and (12) form a boundary value problem for the dependent variables (A, G, H, T, Y_k). The gas-phase kinetics library provides the reaction rates and thermodynamic properties, while the transport package evaluates the transport properties for these equations. Discretization of the differential equations uses conventional finite differencing techniques for nonuniform mesh spacing. Diffusive terms use central differences, with truncation error that is second-order in the mesh spacing. For better convergence, convective terms use upwind differencing, which uses the sign of the velocity to choose the direction of the spatial difference.

2.2 Biogas Electrochemical Oxidation in SOFC. The numerical model, which has been implemented in MATLAB using a
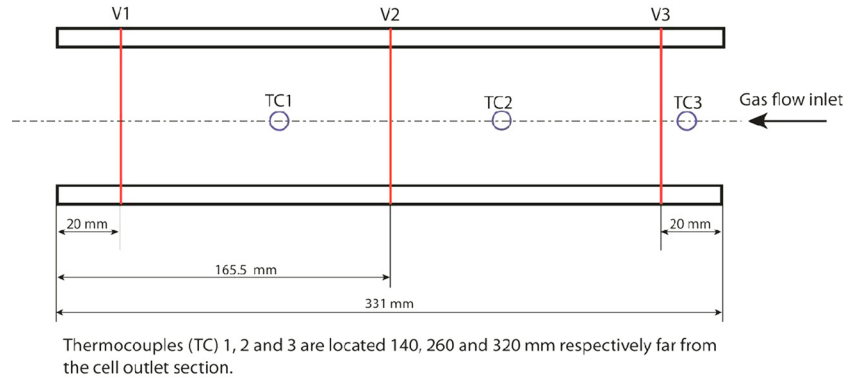
Fig. 2 Geometry of a tubular SOFC

CANTERA interface, aims to describe the biogas energy utilization in an anode-supported SOFC and evaluate its effectiveness.[2] The model considers the biogas reforming process and subsequent electrochemical oxidation occurring inside the anode channel of a tubular, anode-supported SOFC. It is based on the discretization of the reaction environment in such a way that improves the computation of mole fractions of species through rapid convergence. Both thermodynamic and electrochemical aspects are considered in order to ensure completeness (Fig. 2).

Since CANTERA was initially developed to study combustion processes, the present model follows the similarity solution approach, which has been used for flames and is based on converting a system into a certain number of cylindrical elements where one-dimensional laws can be applied. If the cylindrical elements are long and thin, the Mach number is much less than unity (and thus pressure is nearly constant), and the boundary conditions are satisfied, the exact flow equations admit a solution where the dependent variables (axial and radial velocity, temperature, and the mass fractions of all chemical species involved) depend on the axial coordinate only, while pressure is expressed as a function of the radial coordinate as follows:

$$P = P_0 + \Lambda \frac{r^2}{2} \tag{13}$$

with Λ being a constant that must be determined as part of the solution.

For conditions where the similarity solution holds, the flow equations reduce to a set of ordinary differential equations in the axial coordinate. This is possible because the gas flow in the fuel channel is considered to be one-dimensional and laminar, neglecting variations of the gas composition in the transverse direction. This is a reasonable approximation, because the fuel channel typically has characteristic diameters less than a centimeter and mean velocities less than 100 cm/s. Under these circumstances, the Reynolds number is on the order of 100 or less. The following equations represent the set of ODEs employed to solve the problem in the axial coordinate. In particular, the continuity and the radial-momentum equations are expressed as follows:

$$\frac{d}{dz}(\rho u) + 2\rho V = 0 \tag{14}$$

$$\rho \frac{dV}{dt} = \frac{d}{dz}\left(\mu \frac{dV}{dz}\right) - \Lambda - \rho u \frac{dV}{dz} - \rho V^2 \tag{15}$$

while the species-conservation and the energy-conservation equations can be, respectively, written as follows, considering the dependency on both the axial coordinate and time:

$$\rho \frac{dY_k}{dt} = -\rho u \frac{dY_k}{dz} - \frac{dJ_k}{dz} + W_k \dot{\omega}_k \tag{16}$$

$$\rho c_p \frac{dT}{dt} = -\rho c_p u \frac{dT}{dz} + \frac{d}{dz}\left(\lambda \frac{dT}{dz}\right) - \sum_k W_k \dot{\omega}_k h_k - \sum_k J_k c_{p,k} \frac{dT}{dz} \tag{17}$$

The convective terms are discretized through an upwind differencing method, while a central differencing method is employed to discretize the diffusion terms. Boundary conditions are applied at $z = 0$ and $z = L$, with u, T, and Y_k being independent of r, and with v being linear in r (v is usually set to zero at the boundaries).

The fluxes J_k can be computed using the mixture-averaged transport model, following Hirschfelder et al. [7] and Coffee and Heimerl [8]. The electrochemical oxidation at the anode is considered to be carried out for hydrogen only. Once the current density i is determined, it is possible to evaluate the molar flux of the gas species from the electrochemical reactions as

$$J_{H_2,a} = -\frac{i}{2F} \tag{18}$$

$$J_{H_2O,a} = \frac{i}{2F} \tag{19}$$

A positive flux at the anode means that mass enters the anode pore space from the anode-electrolyte three-phase boundary.

The molar production rates $\dot{\omega}_k$ are evaluated using a heterogeneous reaction mechanism (Table 1). Since the mechanism is formulated in terms of elementary reactions on the catalyst surface, the reaction rates depend both on the concentrations of the gaseous reactants and on the coverages of the surface species representing reactive surface sites and adsorbates. In particular, the surface coverage of a species j may be defined as the fraction of an electrode surface covered by the adsorbed species j. Since these coverages are not known a priori, they must be determined as part of the solution.

Unlike the gaseous species, the surface species are effectively immobile on length scales larger than an individual catalyst particle. Therefore, at steady state, the surface coverages must take on values such that the net production rate due to chemistry is zero for every surface species:

$$\dot{\omega}_{surf,k} = 0 \quad k = 1,...,K_s \tag{20}$$

The net production rate of any species (gas or surface) in reaction j is given by

$$\dot{\omega}_k = \sum_j \nu_{k,j} q_j \tag{21}$$

where q_j is the rate of reaction j. The reaction rates are computed assuming mass-action kinetics, with temperature-dependant rate coefficients in Arrhenius form [5]

Table 1 Heterogeneous reaction mechanism for methane reforming on nickel-based catalysts

No	Reaction	A^{a}	n	E^{a}	$\varepsilon_{CO(s)}$
1	$H_2 + (Ni) + (Ni) \rightarrow H(Ni) + H(Ni)$	$1.000 \cdot 10^{-02b}$	0.0	0.0	—
2	$H(Ni) + H(Ni) \rightarrow H_2 + (Ni) + (Ni)$	$2.545 \cdot 10^{+19}$	0.0	81.2	—
3	$O_2 + (Ni) + (Ni) \rightarrow O(Ni) + O(Ni)$	$1.000 \cdot 10^{-02b}$	0.0	0.0	—
4	$O(Ni) + O(Ni) \rightarrow (Ni) + (Ni) + O_2$	$4.283 \cdot 10^{+23}$	0.0	474.9	—
5	$CH_4 + (Ni) \rightarrow CH_4(Ni)$	$8.000 \cdot 10^{-03b}$	0.0	0.0	—
6	$CH_4(Ni) \rightarrow (Ni) + CH_4$	$8.705 \cdot 10^{+15}$	0.0	37.5	—
7	$H_2O + (Ni) \rightarrow H_2O(Ni)$	$1.000 \cdot 10^{-01b}$	0.0	0.0	—
8	$H_2O(Ni) \rightarrow (Ni) + H_2O$	$3.732 \cdot 10^{+12}$	0.0	60.8	—
9	$CO_2 + (Ni) \rightarrow CO_2(Ni)$	$1.000 \cdot 10^{-05b}$	0.0	0.0	—
10	$CO_2(Ni) \rightarrow (Ni) + CO_2(Ni)$	$6.447 \cdot 10^{+07}$	0.0	26.0	—
11	$CO + (Ni) \rightarrow CO(Ni)$	$5.000 \cdot 10^{-01b}$	0.0	0.0	—
12	$CO(Ni) \rightarrow (Ni) + CO(Ni)$	$3.563 \cdot 10^{+11}$	0.0	111.3	-50.0^{c}
13	$O(Ni) + H(Ni) \rightarrow OH(Ni) + (Ni)$	$5.000 \cdot 10^{+22}$	0.0	97.9	—
14	$OH(Ni) + (Ni) \rightarrow O(Ni) + H(Ni)$	$1.781 \cdot 10^{+21}$	0.0	36.1	—
15	$OH(Ni) + H(Ni) \rightarrow H_2O(Ni) + (Ni)$	$3.000 \cdot 10^{+20}$	0.0	42.7	—
16	$H_2O(Ni) + (Ni) \rightarrow OH(Ni) + H(Ni)$	$2.271 \cdot 10^{+21}$	0.0	91.8	—
17	$OH(Ni) + OH(Ni) \rightarrow O(Ni) + H_2O(Ni)$	$3.000 \cdot 10^{+21}$	0.0	100.0	—
18	$O(Ni) + H_2O(Ni) \rightarrow OH(Ni) + OH(Ni)$	$6.373 \cdot 10^{+23}$	0.0	210.9	—
19	$O(Ni) + C(Ni) \rightarrow CO(Ni) + (Ni)$	$5.200 \cdot 10^{+23}$	0.0	148.1	—
20	$CO(Ni) + (Ni) \rightarrow O(Ni) + C(Ni)$	$1.354 \cdot 10^{+22}$	-3.0	116.1	—
21	$O(Ni) + CO(Ni) \rightarrow CO_2(Ni) + (Ni)$	$2.000 \cdot 10^{+19}$	0.0	123.6	—
22	$CO_2(Ni) + (Ni) \rightarrow O(Ni) + CO(Ni)$	$4.653 \cdot 10^{+23}$	-1.0	89.3	—
23	$HCO(Ni) + (Ni) \rightarrow CO(Ni) + H(Ni)$	$3.700 \cdot 10^{+21}$	0.0	0.0	—
24	$CO(Ni) + H(Ni) \rightarrow HCO(Ni) + (Ni)$	$4.019 \cdot 10^{+20}$	-1.0	132.2	—
25	$HCO(Ni) + (Ni) \rightarrow O(Ni) + CH(Ni)$	$3.700 \cdot 10^{+24}$	-3.0	95.8	—
26	$O(Ni) + CH(Ni) \rightarrow HCO(Ni) + (Ni)$	$4.604 \cdot 10^{+20}$	0.0	110.0	—
27	$CH_4(Ni) + (Ni) \rightarrow CH_3(Ni) + H(Ni)$	$3.700 \cdot 10^{+21}$	0.0	57.7	—
28	$CH_3(Ni) + H(Ni) \rightarrow CH_4(Ni) + (Ni)$	$6.034 \cdot 10^{+21}$	0.0	61.6	—
29	$CH_3(Ni) + (Ni) \rightarrow CH_2(Ni) + H(Ni)$	$3.700 \cdot 10^{+24}$	0.0	100.0	—
30	$CH_2(Ni) + H(Ni) \rightarrow CH_3(Ni) + (Ni)$	$1.293 \cdot 10^{+23}$	0.0	55.3	—
31	$CH_2(Ni) + (Ni) \rightarrow CH(Ni) + H(Ni)$	$3.700 \cdot 10^{+24}$	0.0	97.1	—
32	$CH(Ni) + H(Ni) \rightarrow CH_2(Ni) + (Ni)$	$4.089 \cdot 10^{+24}$	0.0	79.2	—
33	$CH(Ni) + (Ni) \rightarrow C(Ni) + H(Ni)$	$3.700 \cdot 10^{+21}$	0.0	18.8	—
34	$C(Ni) + H(Ni) \rightarrow CH(Ni) + (Ni)$	$4.562 \cdot 10^{+22}$	0.0	161.1	—
35	$O(Ni) + CH_4(Ni) \rightarrow CH_3(Ni) + OH(Ni)$	$1.700 \cdot 10^{+24}$	0.0	88.3	—
36	$CH_3(Ni) + OH(Ni) \rightarrow O(Ni) + CH_4(Ni)$	$9.876 \cdot 10^{+22}$	0.0	30.4	—
37	$O(Ni) + CH_3(Ni) \rightarrow CH_2(Ni) + OH(Ni)$	$3.700 \cdot 10^{+24}$	0.0	130.1	—
38	$CH_2(Ni) + OH(Ni) \rightarrow O(Ni) + CH_3(Ni)$	$4.607 \cdot 10^{+21}$	0.0	23.6	—
39	$O(Ni) + CH_2(Ni) \rightarrow CH(Ni) + OH(Ni)$	$3.700 \cdot 10^{+24}$	0.0	126.8	—
40	$CH(Ni) + OH(Ni) \rightarrow O(Ni) + CH_2(Ni)$	$1.457 \cdot 10^{+23}$	0.0	47.1	—
41	$O(Ni) + CH(Ni) \rightarrow C(Ni) + OH(Ni)$	$3.700 \cdot 10^{+21}$	0.0	48.1	—
42	$C(Ni) + OH(Ni) \rightarrow O(Ni) + CH(Ni)$	$1.625 \cdot 10^{+21}$	0.0	128.6	—

[a]Arrhenius parameters for the rate constants written in the form: $k = AT^n \exp(-E/RT)$. The units of A are given in terms of moles, centimeters, and seconds. E is in kJ/mol.
[b]Sticking coefficient.
[c]Coverage-dependent activation energy. Total available surface density Γ is expressed in mol/cm^2 and represents the tuning parameter.

$$k_i = A_i T^n \exp(-E_i/RT) \tag{22}$$

The *heterogeneous reaction mechanism* is partly extracted from Refs. [9–11]. Nickel is the most common anode material (in Ni-YSZ cermets) and is certainly cost-effective. Although there are several crucial issues associated with nickel in reforming reactors (carbon deposition, pore blocking, and deactivation on nickel are well-known problems), there is considerable evidence that SOFCs can use nickel anodes effectively. For instance, nickel is successfully used as a catalyst for hydrocarbon reforming and shifting to produce syngas (a mixture of hydrogen and carbon monoxide). The reactions of methane on nickel have been extensively studied for decades, and different reaction mechanisms and corresponding models have been proposed. Recently, attention has been focused on developing a multistep reaction mechanism based on the knowledge of the elementary steps.

The reaction mechanism reported in Table 1 consists of 42 irreversible reactions among 6 gas-phase and 12 additional adsorbed species.

Most reaction rates are represented in Arrhenius form or as a sticking coefficient. However, the net reaction rates of reactions 12, 20, 21, and 23 depend on the carbon-monoxide coverage $\theta_{CO(s)}$ in the form

$$k = AT^n \exp\left(-\frac{E}{RT}\right) \exp\left(-\frac{\varepsilon_{CO(s)} \theta_{CO(s)}}{RT}\right) \tag{23}$$

Although the reaction mechanism is written as pairs of irreversible reactions, the reverse rate coefficients depend on the forward rate coefficients and the thermodynamics. The reverse rate coefficients are computed to ensure thermodynamic consistency and an asymptotic approach to the equilibrium state.

Elementary reaction mechanisms can be applied more generally than global mechanisms, which may be validated only for specific geometric configurations and operating conditions. The mechanism here was initially developed and validated using nickel-coated honeycomb monoliths for the temperature range from 700 to 1300 K. The validation is based on comparing measured product composition with results of two-dimensional reacting flow simulations for a single channel [9]. In addition to the monolith-based validation, the mechanism reported in Table 1 has been

recently validated in specifically designed experiments using porous Ni-YSZ anode structures [10]. These experiments consider both steam and dry reforming of methane.

Because the reaction mechanism is based on elementary molecular processes, it represents all the global processes in an SOFC anode, including steam reforming of CH_4 to CO and H_2, water-gas-shift reactions, and surface coverage. The mechanism includes surface-adsorbed carbon C(Ni) and oxygen on the surface up to one monolayer O(Ni). However, the mechanism has not been specifically validated for conditions where coking and bulk-phase nickel oxidation occur.

The model described in the present work incorporates the heterogeneous chemistry in Table 1. The mechanism was taken from Ref. [11] and manually modified from the CHEMKIN to CANTERA format. In order to do this, information about mechanism files contained in Dalle Nogare's work was used [12].

Input parameters include pressure, temperature (considered constant in the present model), nearly constant in reality), current applied to the cell, a shape function (optional) to define the current profile, and fluxes of all chemical species entering the anode. The cell-geometry parameters include anode channel length, anode channel radius, anode thickness, and the number of cells for the axial and radial discretization.

The anode thickness is not used to study the phenomena occurring within the anode, but it is considered to be such an extension of the anode radius. This is an approximation used to improve chemical processes occurring within the anode channel, since the present model focuses on the phenomena occurring inside the fuel channel only.

The fuel channel is divided into a certain number of axial cells and every cell is analyzed along the radial coordinate only. The solution is computed by using a cycle, whose number of iterations equals the number of axial cells. Initial gas composition is updated at every iteration with the final results coming from the previous cell. This implies that the transport in the axial direction is predominantly due to diffusion, while that in the radial is due to convection. Moreover, since the present study does not consider a porous medium, the anode reacting surface is assumed to be an interface between the anode and the fuel channel.

Once the boundaries are set, the stack object is solved for every cell by first solving the energy equation and then by turning on all surface chemistry reactions. It is possible to speed up the computation by defining tolerances for both the steady-state problem and for time stepping, while the radial grid can be refined by setting more stringent refinement criteria if needed. Net production rates of all chemical species are computed directly using the mechanism file, while production and destruction rates due to the current applied to the fuel cell are computed by exploiting Faraday's law.

3 Biogas Combustion in Premixed Flames and Electrochemical Oxidation: Comparison

3.1 Emission Comparison. A standard biogas composition (60%CH_4/40%CO_2) has been considered in the calculations. The biogas contaminants (present in traces, as siloxanes and halocarbons) have been neglected. In the case of sulphur, its content in a biogas stream (e.g., from waste water treatment units) can vary from 60 to 200 ppm (for large plants with digesters treated with iron oxides) to 500 ppm (for small farm plants). The sulfur content has a very high impact on the SOFC anodes based on Ni, and it is therefore carefully separated from the biogas, using cleaning guard beds (usually composed of ZnO beds or activated carbons guard beds). For this reason, we did not consider the sulfur content in the biogas, for both PPF and SOFC analysis.

3.1.1 Partial Premixed Flames. The counter flow flame model described above, along with the Chemkin library, was employed to analyze the emissions of pollutants for biogas-air partially premixed flames. Figure 3 shows the mole fraction profiles of the main pollutant species. The biogas composition is assumed to be 60%CH_4/40%CO_2 (reference case). The distance between the two nozzles is 2 cm, the pressure is 1 atm, and the inlet temperature is set to 300 K for both the fuel (left) and the oxidizer (right) streams. Note that for partially premixed flames, the main parameters of interest are the equivalence ratio (ϕ) of the fuel stream and the strain rate. As indicated in Table 2, simulation results are shown for $\phi = 1.4$ and 3.0 (values commonly used in current combustion literature [1]), and strain rates of $150 \, s^{-1}$ and $200 \, s^{-1}$ (in order to assure relatively high inlet velocities).

Since Chemkin opposed-flow-flame model does not allow the user to directly specify ϕ at the fuel nozzle, a useful way is to specify the mole fractions of all chemical species at the fuel nozzle for a given ϕ. Similarly, the global strain rate is specified by computing the inlet densities and velocities for both the fuel and oxidizer using the following two equations [13]:

$$a_s = \frac{2|v_O|}{L}\left(1 + \frac{|v_F|}{|v_O|}\sqrt{\frac{\rho_F}{\rho_O}}\right) \qquad (24)$$

where a_s represents the global strain rate, and:

$$\rho_O v_O^2 = \rho_F v_F^2 \qquad (25)$$

Figure 3 shows the effect of strain rate (a_s) and equivalence ratio (ϕ) on the flame structure and emissions. As the strain rate is increased, the emissions of pollutants are significantly reduced. In particular, the CO and CO_2 peaks decrease slightly, while the NO_x (NO+NO_2) peaks show a considerable reduction. There is similar reduction in the peak mole fraction of C_2H_2, which is known to be a good precursor for soot formation. Regarding the effect of ϕ, results indicate that for richer mixtures the emission peaks are shifted towards the air nozzle. In addition, the CO and CO_2 peaks are considerably reduced, while the NO_x production is enhanced, as well as the soot formation, which is indicated by the higher C_2H_2 peak.

3.1.2 SOFC Electrochemical Oxidation. The electrochemical-oxidation model described above along with the heterogeneous-reaction mechanism (Table 1) was employed to analyze the emissions and the effectiveness of biogas electrochemical oxidation, with simultaneous reforming processes, occurring inside the anode channel of a tubular SOFC. The anode-channel length is 331 mm, the inner diameter is 10.5 mm, and the anode thickness is 1.7 mm. Biogas composition is taken as the same as that used in flame studies, i.e., 60%CH_4/40%CO_2.

Figure 4 shows the predicted mole fraction profiles of the main chemical species along the fuel (anode) channel for two different open circuit voltage (OCV) cases, i.e., without electrochemical reactions. The cell temperature is set to 800 °C, CH_4 mass flow rate is 50 ml/min, while CO_2-to-biogas ratio is set to 1.0 and 1.5, respectively, which yields the CO_2 mass flow rate.

For both cases, results indicate a rapid consumption of CH_4 and CO_2 through Ni-catalyzed dry reforming, and consequent production of H_2 and CO. Also, a small amount of water is formed, which is due to the occurrence of the inverse water gas-shift reactions. In both cases, chemical equilibrium is approached but not achieved, even though dry reforming seems to proceed rapidly, especially in the first half of the fuel channel.

Figure 5 shows the predicted mole fraction profiles of the main chemical species along the fuel channel when a current load of 15 A is applied to the cell, i.e., with electrochemical reactions. The cell temperature is set to 800 °C again, CH_4 mass flow rate is 53 ml/min and the fuel utilization (FU) factor is 50%, while CO_2-to-biogas ratio is set to 1.0.

For this case, the amount of H_2O formed is more pronounced compared to the OCV case, which is due to the electrochemistry of the cell. For the reason, some CO is also consumed in the later part of the cell, forming CO_2 by reacting with H_2O through direct water shift driven by the high H_2O molar fraction. The H_2O
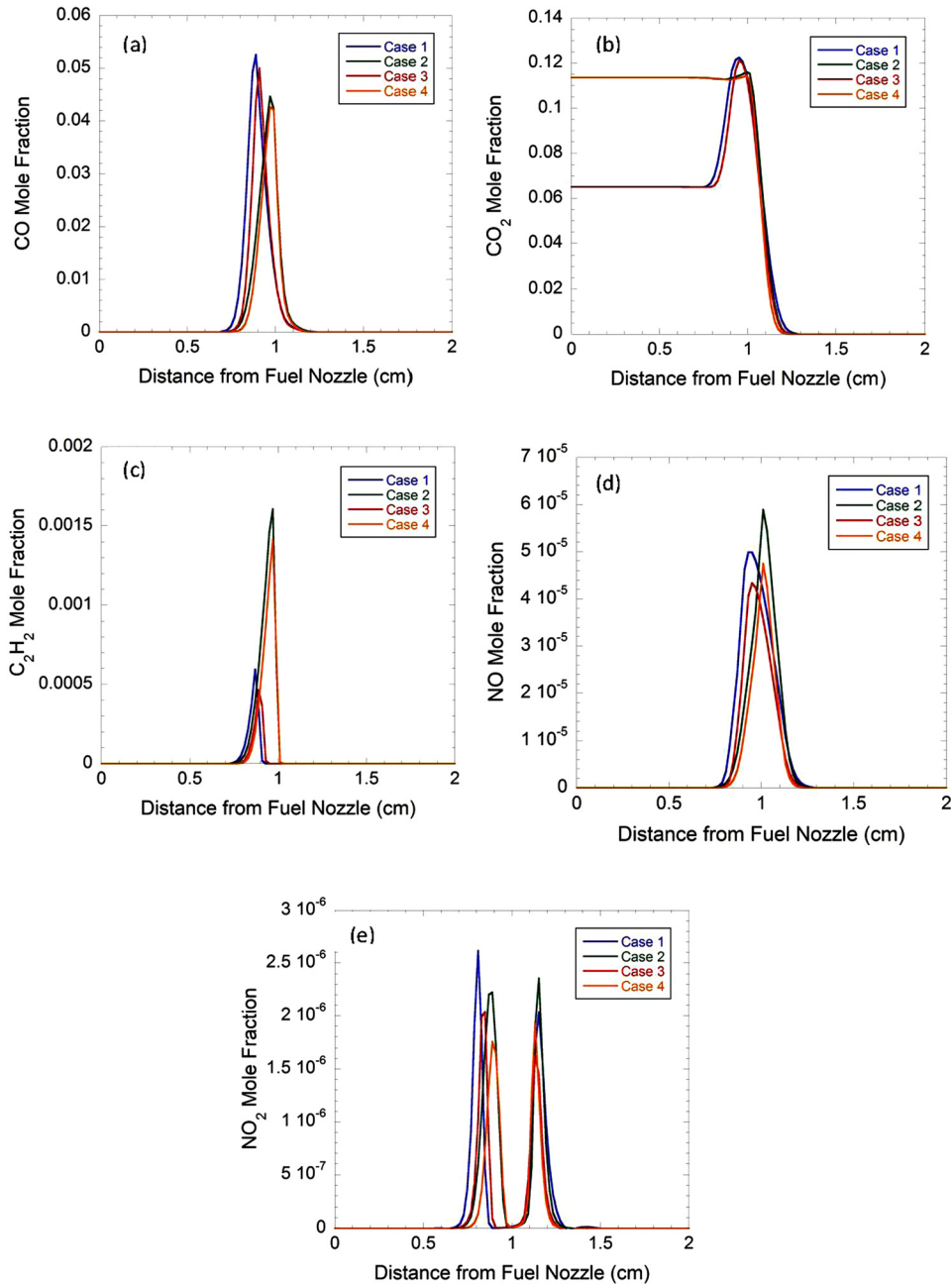
Fig. 3   Effect of strain-rate and equivalence ratio on biogas-air counter-flow flames: (*a*) CO, (*b*) CO_2, (*c*) C_2H_2, (*d*) NO, (*e*) NO_2 profiles

Table 2   Strain rate and equivalence ratio values for the four simulated partially premixed flames

Case	Strain rate	Equivalence ratio
1	$150\,s^{-1}$	1.4
2	$150\,s^{-1}$	3.0
3	$200\,s^{-1}$	1.4
4	$200\,s^{-1}$	3.0

profile remains monotonic because of its continuous electrochemical production (from the H_2 produced by the CO shift in CO_2) along the cell at constant current. CH_4 is consumed by both steam and dry reforming, which consume H_2O and CO_2, respectively, to produce H_2 (primary fuel of the electrochemical reaction) and CO. H_2 is consumed to produce current, but at the same time, it is produced through water gas shift reaction, consuming CO and H_2O and producing CO_2. The CO is consumed by the water gas shift reaction, which produces H_2 (electrochemically oxidized in water) and CO_2. The H_2O is consumed by the steam reforming and water gas shift reactions, but is produced by the H_2 electrochemical oxidation. The same reactions operate in case of CO_2-to-biogas ratios of 1.0 and 1.5, as clearly indicated by the highest amount of CO_2 in the exhaust gases.

Therefore, balances between all chemical processes involved in such a mechanism are usually extremely difficult to be established because of the overall complexity, but they may provide researchers with interesting data in order to better investigate the overall cell chemical behavior.

3.1.3   Comparison of Emissions. The PPF exhaust contains significant amounts of NO_x and C_2H_2, which are precursors of atmosphere pollution, while the SOFC exhaust stream does not
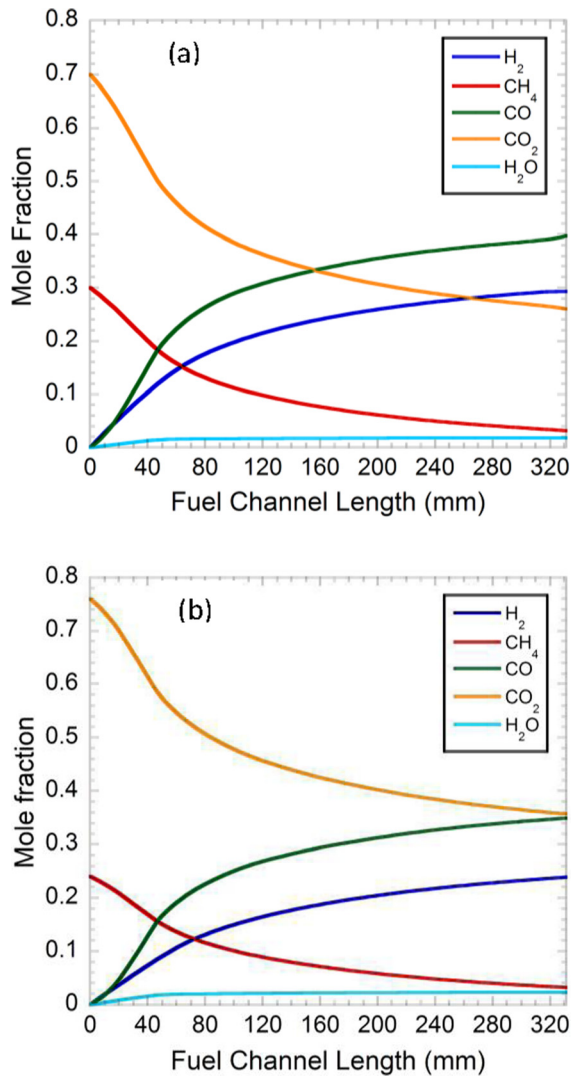
Fig. 4 Predicted mole fraction profiles of major chemical species when CO_2-to-biogas ratio is set to (a) 1.0 and (b) 1.5 (open circuit voltage configuration)

Fig. 5 Predicted mole fraction profiles of major chemical species when CO_2-to-biogas ratio is set to (a) 1.0 and (b) 1.5 (I = 15 A, FU = 50%)

contain such chemical species due to the absence of combustion reactions. In terms of other major components, the PPF exhaust stream is mainly composed of N_2, along with CO and CO_2. If depurated by the N_2 content, the stream has a molar fraction of 7.7% CO and 37.4% CO_2. The SOFC exhaust stream has no N_2, and mainly contains CO and CO_2, due to the biogas reforming process, with their mole fractions being 12.5% and 50.1% (mainly coming from the biogas reforming process to prevent C deposits on the anode), respectively, for the reference case of CO_2-to-biogas ratio of 1.0. Therefore, the PPF exhaust has a lower absolute content of CO and CO_2, but they are immersed in a amount of N_2, which increases the energy costs for the separation of these species from the exhaust stream.

In conclusion, the use of biogas in PPFs produces direct pollutant species, and a lower amount of CO_2 and CO, which are, however, difficult to separate from the stream.

3.2 Exergy Comparison. A given primary fuel can be used along different energy pathways involving different transformation processes depending upon the application. The energy product(s) of the transformation chain will be different in quantity and form (e.g., mechanical power, heat flow at a given temperature, a stream of different chemical composition, etc.). Consequently, the comparison of different energy pathways may be strongly affected
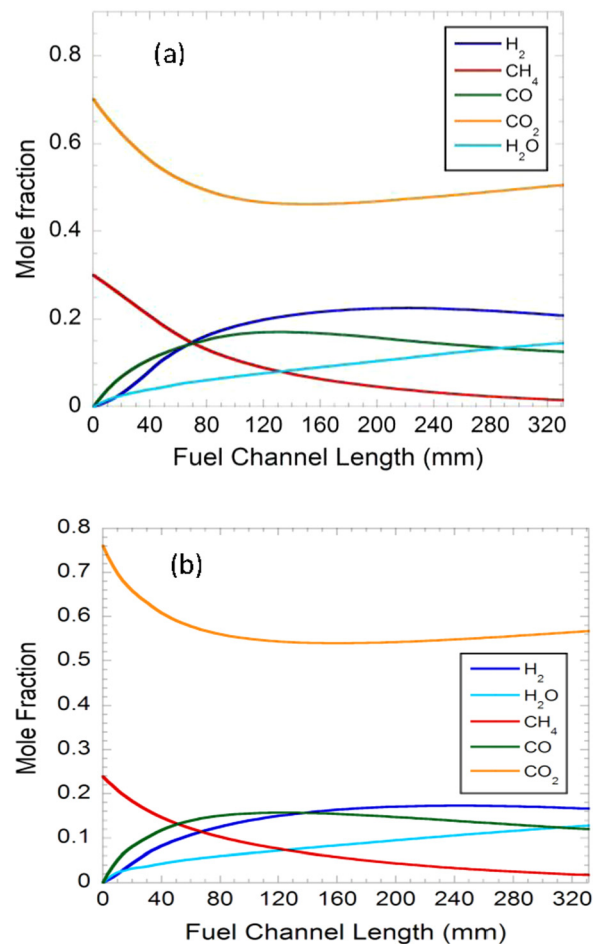
by the differences in the nature of the energy products, and, thus, may only be qualitative. In this context, a thermodynamic approach based on the concept of exergy can homogenize different type of energy flows, and allow a quantitative comparison of the energy pathways. Therefore, this approach is utilized in the present study. The same primary fuel (biogas) with a given exergy content (chemical exergy), is used in two different transformation pathways, i.e.,

1. Combustion in partially premixed flames, producing heat flow at a given (high) temperature and a stream of chemical species at a given thermodynamic state.
2. Electrochemical oxidation in SOFC, producing electric power and a stream of chemical species at given thermodynamic state.

The comparison between the two energy transformation pathways will therefore be done using the exergy analysis.

3.2.1 Basic Considerations in Exergy Analysis. Consider an open system, which exchanges mass flows G_k, thermal flows Φ_{qj} and mechanical-electric power W_t. The exergy equation in terms of power can be expressed as

$$\sum_{j=1}^{N} \Psi_{qj} - W_t = \left(\frac{dA^t}{dt}\right)_{VC} + \sum_{k=1}^{NC} \pm G_k \cdot b_k^t + \Psi_I \quad (26)$$

where the terms are the exergy of thermal flow: $\Psi_{qj} = \Phi_{qj} \cdot (1 - T_0/T_j)$, the total internal exergy: $A^t = (A) + (E_c + E_p) = (U + p_0 \cdot V - T_0 \cdot S) + (E_c + E_p)$, the total

Table 3 Fuel, product and exergy efficiency of the four PPF cases with (1) $a_s = 150\,s^{-1}$, $\phi = 1.4$, (2) $a_s = 150\,s^{-1}$, $\phi = 3.0$, (3) $a_s = 200\,s^{-1}$, $\phi = 1.4$, (4) $a_s = 200\,s^{-1}$, $\phi = 3.0$

Case 1: Strain rate $150\,s^{-1}$—Equivalence ratio 1.4

Fuel

CH$_4$ (%)			CO$_2$ (%)			T (K)	p (bar)	b (kJ/kg)	G (kg/s)	Exergy (kW)
60			40			298.15	1.013	18464.33	1.59 10^{-4}	2.941

Product

Exhaust data

O$_2$ (%)	CO$_2$ (%)	N$_2$ (%)	H$_2$ (%)	CO (%)	H$_2$O (%)	T (K)	p (bar)	b (kJ/kg)	G (kg/s)	Exergy (kW)
1.09	12.24	66.45	0.76	2.52	16.15	1877.23	1.013	1577.13	3.09 10^{-4}	0.475

Thermal flow data

Heat flow (kW)	Temperature (K)	Exergy (kW)
0.0634	1877.23	0.053

Exergy efficiency

Fuel (kW)	Product (kW)	Exergy efficiency
2.941	0.528	0.179

Case 2: Strain rate $150\,s^{-1}$—Equivalence ratio 3.0

Fuel

CH$_4$ (%)			CO$_2$ (%)			T (K)	p (bar)	b (kJ/kg)	G (kg/s)	Exergy (kW)
60			40			298.15	1.013	18464.33	1.59 10^{-4}	2.941

Product

Exhaust data

O$_2$ (%)	CO$_2$ (%)	N$_2$ (%)	H$_2$ (%)	CO (%)	H$_2$O (%)	T (K)	p (bar)	b (kJ/kg)	G (kg/s)	Exergy (kW)
0.99	11.64	65.84	1.17	3.78	16.01	1843.75	1.013	1696.72	3.09 10^{-4}	0.511

Thermal flow data

Heat flow (kW)	Temperature (K)	Exergy (kW)
0.049	1843.65	0.041

Exergy efficiency

Fuel (kW)	Product (kW)	Exergy efficiency
2.941	0.552	0.188

Case 3: Strain rate $200\,s^{-1}$—Equivalence ratio 1.4

Fuel

CH$_4$ (%)			CO$_2$ (%)			T (K)	p (bar)	b (kJ/kg)	G (kg/s)	Exergy (kW)
60			40			298.15	1.013	18464.33	2.12 10^{-4}	3.922

Product

Exhaust data

O$_2$ (%)	CO$_2$ (%)	N$_2$ (%)	H$_2$ (%)	CO (%)	H$_2$O (%)	T (K)	p (bar)	b (kJ/kg)	G (kg/s)	Exergy (kW)
1.08	12.11	66.24	0.83	2.85	16.07	1853.01	1.013	1590.44	4.07 10^{-4}	0.647

Thermal flow data

Heat flow (kW)	Temperature (K)	Exergy (kW)
0.0694	1853.01	0.058

Exergy efficiency

Fuel (kW)	Product (kW)	Exergy efficiency
3.922	0.706	0.180

Case 4: Strain rate $200\,s^{-1}$—Equivalence ratio 3.0

Fuel

CH$_4$ (%)			CO$_2$ (%)			T (K)	p (bar)	b (kJ/kg)	G (kg/s)	Exergy (kW)
60			40			298.15	1.013	18464.33	1.95 10^{-4}	3.595

Product

Exhaust data

O$_2$ (%)	CO$_2$ (%)	N$_2$ (%)	H$_2$ (%)	CO (%)	H$_2$O (%)	T (K)	p (bar)	b (kJ/kg)	G (kg/s)	Exergy (kW)
1.24	11.45	65.95	1.16	3.78	15.81	1824.14	1.013	1675.39	4.07 10^{-4}	0.682

Thermal flow data

Heat flow (kW)	Temperature (K)	Exergy (kW)
0.0552	1824.14	0.046

Exergy efficiency

Fuel (kW)	Product (kW)	Exergy efficiency
3.595	0.728	0.203

specific exergy of mass flow: $b^t = (b) + (e_c + e_p)$, and the exergy destroyed by irreversibility Ψ_I.

The total specific exergy of a mass flow b_t is composed of 4 terms: kinetic, potential, physical and chemical specific exergy. Both the kinetic and potential exergy are usually negligible in the majority of exergy calculations in real industrial systems.

The physical exergy b_{ph} is the amount of work which can be recovered from the mass flow when it performs a reversible transformation from its starting thermodynamic state (T, p) and ending in a final state at thermal and mechanical equilibrium with the reference state (T_0, p_0), without modification of its chemical composition. The expression for the specific physical exergy of a mass flow is:

$$b_{ph} = (h - h_0) - T_0 \cdot (s - s_0) \tag{27}$$

The chemical exergy is related to a transformation of the mass flow: from the starting state (where the mass flow is in thermal

Case 1: CO_2-to-biogas ratio set to 1.0 (I = 15 A, FU = 50%)

FUEL

CH$_4$ (%)	CO$_2$ (%)	T (K)	p (bar)	b (kJ/kg)	G (kg/s)	Exergy (kW)
30	70	298.15	1.013	7336.49	0.004700	34.394

Product — Exhaust data

CH$_4$ (%)	CO$_2$ (%)	H$_2$ (%)	CO (%)	H$_2$O (%)	T (K)	p (bar)	b (kJ/kg)	G (kg/s)	Exergy (kW)
2.0	50.1	20.5	12.5	15.0	1073.15	1.013	4157.24	0.004704	19.555

Electric power data

Current (A)	Voltage (V)	Electric power (kW)	Exergy (kW)
75	0.761	0.0570	0.0571

Exergy efficiency

Fuel (kW)	Product (kW)	Exergy efficiency
34.394	19.612	0.570

Case 1: CO_2-to-biogas ratio set to 1.5 (I = 15 A, FU = 50%)

Fuel

CH$_4$ (%)	CO$_2$ (%)	T (K)	p (bar)	b (kJ/kg)	G (kg/s)	Exergy (kW)
24	76	298.15	1.013	5711.59	0.006100	35.008

Product — Exhaust data

CH$_4$ (%)	CO$_2$ (%)	H$_2$ (%)	CO (%)	H$_2$O (%)	T (K)	p (bar)	b (kJ/kg)	G (kg/s)	Exergy (kW)
2.0	57.0	16.0	12.0	13.0	1073.15	1.013	3534.27	0.006135	21.685

Electric power data

Current (A)	Voltage (V)	Electric power (kW)	Exergy (kW)
75	0.752	0.0564	0.0564

Exergy efficiency

Fuel (kW)	Product (kW)	Exergy efficiency
35.008	21.741	0.621

and mechanical equilibrium with the reference state, but not in chemical equilibrium: it is therefore in the *restricted dead state*) to the ending state, which is the reference state of the environment with the chemical composition of the biosphere (it is therefore the *dead state*). The modification of chemical exergy occurs in case of chemical or electrochemical reactions in the mass flow. For a stream composed of a mixture of chemical species, the expression for the chemical exergy is as follows:

$$\overline{b}_{ch}(T_0, p_0) = \sum_i y_{i,0} \cdot \overline{b}_{ch,i}(T_0, p_{1,0}) + \overline{R} \cdot T_0 \cdot \sum_i y_{i,0} \cdot \ln y_{i,0} \tag{28}$$

where subscript "0" refers to the "restricted dead state". In general, for any substance, chemical exergy $\overline{b}_{ch,i}(T_0, p_{1,0})$ can be obtained from thermodynamic tables. The chemical exergy of a chemical species not present in the chemical composition of the dead state, for example, fuel is

$$\overline{b}_{ch,\text{fuel}}(T_0, p_0) = -\Delta \overline{g}_{\text{reaction}}(T_0, p_0)$$
$$+ \left[\sum_P \frac{n_P}{n_{\text{fuel}}} \cdot \overline{b}_{ch,P} - \sum_{R \neq \text{fuel}} \frac{n_R}{n_{\text{fuel}}} \cdot \overline{b}_{ch,R} \right] \tag{29}$$

where the considered reaction sets the atoms of the chemical species in their final equilibrium composition in the dead state. For instance, the considered reaction in case of a hydrocarbon fuel is the oxidation which takes C atoms in equilibrium in the form of CO_2, and H atoms in the form of H_2O.

3.2.2 Exergy Analysis: Partially Premixed Flames.
For the exergy analysis, we consider the same four cases as those for the analysis of emissions: PPFs with (1) strain rate $a_s = 150\,\text{s}^{-1}$, equivalence ration $\phi = 1.4$, (2) $a_s = 150\,\text{s}^{-1}$, $\phi = 3.0$, (3)

$a_s = 200\,\text{s}^{-1}$, $\phi = 1.4$, and (4) $a_s = 200\,\text{s}^{-1}$, $\phi = 3.0$. In the exergy analysis, the fuel and the product are considered as follows:

- Fuel: total exergy (physical + chemical) of the PPF inlet fuel stream (the exergy of the air inlet stream is zero)
- Product: total exergy (physical + chemical) of the PPF outlet exhaust stream + exergy of the thermal power produced

The data concerning the fuel, product and exergy efficiency for the four analysed cases are reported in Table 3.

Since the specific exergy value of the fuel stream is the same for all the four cases, the exergy efficiency depends only on the product. In general, the cases with higher strain rate (cases (3) and (4)) show higher exergy efficiency. This is due to higher heat flow rate (although at slightly lower temperature), while the exergy content of the exhaust stream is quite similar due to similar composition. In general, the cases with higher ϕ (cases (2) and (4)) show higher exergy efficiency, which this is due to higher exergy content of the exhaust stream, as a result of higher H$_2$ and CO content.

Therefore, an important observation here is that feeding with higher strain rate and especially with richer mixture leads to better exergy balance. Of course, to be exploited, this requires further use of the exhaust stream in order to recover its chemical exergy content.

3.2.3 Exergy Analysis: SOFC Electrochemical Oxidation.
For the exergy analysis, we again consider the same cases as analyzed for emissions: CO_2-to-biogas ratio of (a) 1.0 and (b) 1.5 (I = 15 A, FU = 50%). In the exergy analysis, the fuel and product are considered as follows:

- Fuel: total exergy (physical + chemical) of the SOFC anode inlet fuel stream (the exergy of the air cathode inlet stream is zero)
- Product: total exergy (physical + chemical) of the SOFC outlet exhaust stream + electric power produced

The data concerning the fuel, product and exergy efficiency of the two analysed cases are reported in Table 4.

Case (b) has a fuel stream with a higher CO_2 content (safer reforming conditions) and exhaust stream composition which is not significantly different from that for case (a). For these conditions, case (b) shows higher efficiency, which is essentially due to lower exergy content of the fuel (higher CO_2 content with lower chemical exergy), while the exergy content of the product, although lower than that in case (a) due to a lower H_2 molar fraction, is not reduced by the same amount. The exergy content of the electric power is quite similar (slightly higher in case (a) due to better composition of the fuel).

In conclusion, the feeding with a safer (in terms of reforming) fuel composition (higher CO_2-content) shows better exergy balance.

In the SOFC cases, the high exergy efficiency values are essentially due to the high residual exergy content of the exhaust streams. However, this requires further use of the exhaust stream in order to recover its chemical exergy content.

3.2.4 Comparison. The utilisation of the biogas fuel for electrochemical oxidation in a SOFC shows higher exergetic efficiency compared to the chemical oxidation in partially premixed flames: exergy efficiency of 0.62 in case of SOFC, compared to 0.20 in case of PPF. This is due to the lower irreversibility in case of the electrochemical reaction compared to the chemical reaction. In particular, this is due to:

- higher exergy value of the energy product of the reaction: electric power in case of SOFC and thermal energy (even if at high temperature) in case of PPF
- especially higher exergy quality of the exhaust stream exiting from the energy device

Thus, the electrochemical oxidation makes better use of the chemical exergy (chemical potential) of the inlet flow, leaving a higher chemical exergy content in the exhaust stream. Of course, as stated earlier, this higher efficiency is based upon further using the exhaust stream in order to recover its chemical exergy content. Therefore, it is important to identify an effective use of the exhaust exergy in a energy device following the SOFC. In contrast, the residual exergy of the PPF is relatively low, indicating higher irreversibility during the transformation of chemical exergy in the PPF process.

4 Conclusions

In the comparison of two pathways to extract chemical exergy from a fuel stream (direct chemical reaction (combustion) versus electrochemical reaction) a powerful instrument based on thermodynamics criteria is the exergy analysis. Nevertheless, the exergetic approach, even if very powerful and "objective," is not complete and is not able to get some other points of high value in the present energy context, as the emission of contaminants in atmosphere. Therefore, the emission analysis could represent a useful complementary approach, in order to outline the "external" effect of a energy transformation pathway. Biogas, a viable renewable fuel which can to be used in both chemical and electrochemical processes to produce energy, has been considered as a fuel for this comparison.

We have performed extensive simulations and analysis of biogas chemical use in partially premixed flames (PPF), and electrochemical use in SOFC cells. Simulations pertaining to the latter use have been validated through comparison with measurements (not shown here, see Ref. [2]).

From an environmental point of view, the PPF exhaust stream has significant traces of NO_x and C_2H_2, which are precursors of atmosphere pollution, while the SOFC exhaust stream does not contain such chemical species due to the absence of combustion. In terms of major constituents, the PPF exhaust stream contains 7.7% CO and 37.4% CO_2 (by volume) in a bath of N_2, while the SOFC exhaust stream contains 12.5% CO and 50.1% CO_2 (mainly from the biogas reforming process to prevent C deposits on the anode), but no N_2. Therefore, the PPF exhaust has a lower absolute content of CO and CO_2, which are immersed in a large molar fraction of N_2, which increases the overall costs for the separation of these species from the exhaust stream.

From a exergy point of view, the utilisation of the biogas in the form of electrochemical oxidation in a SOFC indicates significantly higher exergetic efficiency compared to the chemical oxidation in partially premixed flames, with the exergy efficiency of 0.62 in case of SOFC compared to 0.20 in case of PPF. This can mainly be attributed to exergy quality of the exhaust stream from the energy device under consideration. This higher efficiency is, however, conditioned on the possibility of further using the exhaust stream and extracting its chemical exergy content.

In conclusion, biogas may be an efficient alternative to conventional methane in both chemical and electrochemical processes, and has the desirable characteristics to play a significant role in the future for both energy pathways.

Nomenclature

Greek Symbols

ρ = density (kg m^{-3})
μ = dynamic viscosity (Pa s)
λ = thermal conductivity (W m^{-1} K^{-1})
Λ = constant
$\dot{\omega}$ = molar net production rate (mol m^{-2} s^{-1})
ν = net stoichiometric coefficient

Symbols

A = Arrhenius pre-exponential factor (A m^{-2})
c_p = specific heat capacity at constant pressure (J kg^{-1} K^{-1})
E = activation energy (J)
F = Faraday constant (C mol^{-1})
h = specific enthalpy (J kg^{-1})
i = current density (A m^{-2})
J = molar flux (mol m^{-2} s^{-1})
K = number of gaseous species
K_s = number of surface species
P = pressure (Pa)
P_0 = reference pressure (Pa)
r = radial coordinate (m)
t = time (s)
T = temperature (K)
u = axial velocity (m s^{-1})
v = radial velocity (m s^{-1})
V = normalized radial velocity (s^{-1})
W = molecular weight (kg kmol^{-1})
X = mole fraction
Y = mass fraction
z = axial coordinate (m)

Indexes

F = fuel
i = reaction

j, k, m = species

O = oxidizer

surf = surface species

Acronyms

FU = fuel utilization

OCV = open circuit voltage

PPF = partially premixed flames

SOFC = solid oxide fuel cell

References

[1] Som, S., and Aggarwal, S. K., 2007, "A Numerical Investigation of Methane Air Partially Premixed Flames at Elevated Pressures," Combust. Sci. Technol., **179**(6), pp. 1085–1112.

[2] Quesito, F., Novaresio, V., Lanzini, A., Santarelli, M., and Beretta, D., "Direct Reforming of Biogas on Ni-Based SOFC Anodes: Modelling of Heterogeneous Reactions and Validation With Experiments," J. Power Sources (submitted).

[3] Kármán, T. V., 1921, "Über laminare und turbulente Reibung," Z. Angew. Math. Mech., **1**(4), pp. 233–252.

[4] Schlichting, H., 1979, *Boundary Layer Theory*, McGraw-Hill, New York.

[5] Evans, G. H., and Grief, R., 1988, "Forced Flow Near a Heated Rotating Disk: A Similarity Solution," Numer. Heat Transfer, **14**(3), pp. 373–387.

[6] Kee, R. J., Miller, J. A., Evans, G. H., and Dixon-Lewis, G., 1989, "A Computational Model of the Structure and Extinction of Strained, Opposed Flow, Premixed Methane-Air Flames," Proceedings of the 22nd Symposium (International) on Combustion, The Combustion Institute, Pittsburgh, PA, pp. 1479–1494.

[7] Hirschfelder, J. O., Curtiss, C. F., and Bird, R. B., 1954, *Molecular Theory of Gases and Liquids*, John Wiley and Sons, New York.

[8] Coffee, T. P., and Heimerl, J. M., 1981, "Transport Algorithms for Premixed, Laminar Steady-State Flames," Combust. Flame, **43**, pp. 273–289.

[9] Zhu, H., Kee, R. J., Janardhanan, V. M., Deutschmann, O., and Goodwin, D. G., 2005, "Modeling Elementary Heterogeneous Chemistry and Electrochemistry in Solid-Oxide Fuel Cells," J. Electrochem. Soc., **152**(12), pp. A2427–A2440.

[10] Hecht, E. S., Gupta, G. K., Zhu, H., Dean, A. M., Kee, R. J., Maier, L., and Deutschmann, O., 2005, "Methane Reforming Kinetics Within a Ni-YSZ SOFC Anode Support," Appl. Catal. A, **295**, pp. 40–51.

[11] DETCHEM, 2012, accessed April, http://www.detchem.com

[12] Dalle Nogare, D., 2008, "Modeling Catalytic Methane Partial Oxidation With Detailed Chemistry," Ph.D. thesis, Dipartimento dei Principi e Impianti dell'Ingegneria Chimica "I. Sorgato," Università degli Studi di Padova, Italy.

[13] Vagelopoulos, C. M., Egolfopoulos, F. N., and Law, C. K., 1994, "Further Considerations on the Determination of Laminar Flame Speeds With the Counterflow Twin-Flame Technique," Proc. Combust. Instit., **25**, pp. 1341–1347.